



## Numerical simulation of creep notched bar of P91 steel

N. Ab Razak

Universiti Malaysia Pahang, Malaysia

[norhaida@ump.edu.my](mailto:norhaida@ump.edu.my)

C. M. Davies

Imperial College London, United Kingdom

[catrin.davies@imperial.ac.uk](mailto:catrin.davies@imperial.ac.uk)

**ABSTRACT.** Numerous components designed for use at elevated temperatures now exhibit multiaxial stress states as a result of geometric modification and material inhomogeneity. It is necessary to anticipate the creep rupture life of such components when subjected to multiaxial load. In this work finite element analysis has been performed to study the influence of different notches, namely blunt and medium notches on the stress distribution across the notch throat during the creep exposure. Within the FE model, a ductility exhaustion model based on the Cocks and Ashby model was utilized to forecast the creep rupture time of notched bar P91 material. The lower and upper bound of creep ductility are employed in the FE analysis. Different notch specimens have different stress and damage distribution. It is shown that for both types of notches, the von Mises stress is lower than the net stress, indicating the notch strengthening effect. The accumulation of creep damage in the minimum cross-section at each element across the notch throat increases over time. The point at which damage first occurs is closer to the notch root for the medium notch than for the blunt notch. The long-term rupture life predicted for blunt notch specimens appears to be comparable to that of uniaxial specimens. The upper bound creep ductility better predicts the rupture life for medium notches.

**KEYWORDS.** P91 steel; Multiaxial stress state; Finite element analysis; Ductility exhaustion model; Cocks and Ashby model.



**Citation:** Ab Razak, N., Davies, C.M., Numerical Simulation of Creep Notched Bar of P91 Steel, *Frattura ed Integrità Strutturale*, 62 (2022) 261-270.

**Received:** 30.03.2022

**Accepted:** 20.06.2022

**Online first:** 29.08.2022

**Published:** 01.10.2022

**Copyright:** © 2022 This is an open access article under the terms of the CC-BY 4.0, which permits unrestricted use, distribution, and reproduction in any medium, provided the original author and source are credited.

## INTRODUCTION

Modern boiler power plant design necessitates a better understanding of the material's high-temperature performance in the presence of a multiaxial state of stress. These stresses are typically caused by geometrical change and material inhomogeneity [1]. In general, uniaxial creep tests are used to investigate mechanical



properties such as creep deformation of a material. However, data on the multiaxial response of the material under static load at elevated temperatures is frequently required for engineering design applications.

The presence of a notch causes a non-uniform multiaxial state of stress, which causes non-uniform creep straining and creep cavitation, resulting in a change in rupture life. The degree and distribution of multiaxiality are dictated by the volume of material surrounding the notch root, which is determined by the notch geometry and material creep ductility [2,3]. The use of an axial notched bar tension test at the laboratory scale helps understand the multiaxial state of stress on creep deformation and failure. The geometry of the notch determines a material's degree of multiaxiality at a given temperature.

Experimental studies have been conducted on the creep deformation and fracture behaviours of notched bar specimens. Goyal [4] experimentally studied the effect of multiaxial stress on a U-type notch made of P91 material and found that the decreasing notch root radius increased the level of constraint. Chang et.al investigate the multiaxial stress state of P92 on uniaxial and notched specimens at 650°C and found that the notch strengthening effect in the presence of a notch [5]. The strengthening effect in the presence of the notch can be observed in the P91 material [6,7], Nimonic 80A[8], 2.25Cr-1Mo [1] and Cr-Mo-V [9]. The strengthening effect was shown to diminish as applied stress decreased and rupture life increased. The creep rupture behavior is to be governed by the von mises stress, maximum principal stress, and hydrostatic stress [10].

In the damage analysis, the reduction in creep ductility under multiaxial stress states should be considered. Creep ductility has shown a clear reduction, particularly at periods longer than 10,000 hours for P91 and P92 material [11–13]. It is suggested that the boron nitride particles cause long-term degradation in creep ductility in P92 material by accelerating the formation of creep voids [13]. Creep ductility shows a strong stress dependency at a wider stress range. The stress-dependent effect of creep ductility on creep crack growth has been investigated, and it is shown that increasing the transition region size of creep ductility increases the transition of creep parameter, C\* region size on da/dt-C\* curves [14]. The results of accelerated testing on a pre-compressed 316H material demonstrate that the creep ductility acquired by accelerated testing can be utilized to forecast long-term creep failure [15].

FE analysis in conjunction with a damage mechanics model has been widely employed for creep damage and rupture life prediction under multiaxial stress states, for example, the Kachanov Robotnov model [5,6,16,17], Spindler model[18,19] and Cock and Ashby model [5,9,20,21]. All these models correlate the ratio of multiaxiality and uniaxial ductility, to the ratio of hydrostatic stress and the equivalent stress which is often known as triaxiality stress. This method has been widely used in creep crack growth prediction [22].

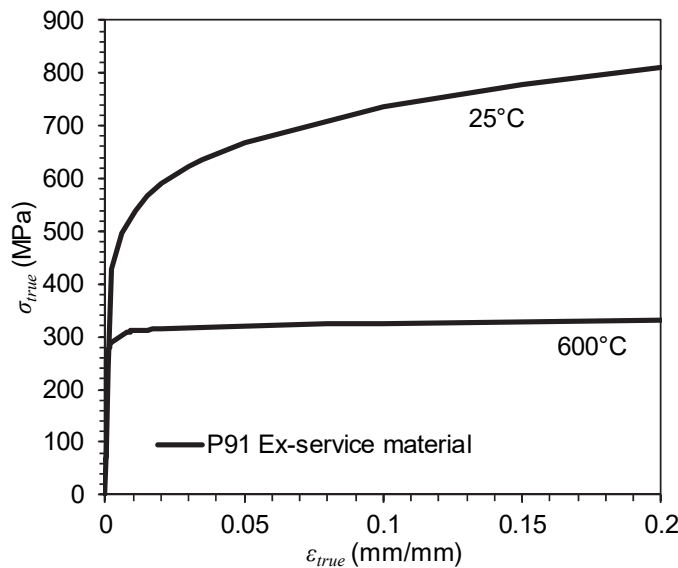


Figure 1: True stress strain behavior of ex-service P91 material tested at 25°C and 600°C

Improving the accuracy of high-temperature components' life evaluation methods is critical for rationalizing component design and life management. Evaluating creep damaging behaviours of materials under multiaxial stress state would result in a rational assessment. In this work, the prediction of creep rupture life under the multiaxial condition has been performed using FE analyses by employing Cocks and Ashby model. Finite element analyses were carried out to study the



influence of notch geometry on the stress distribution across the notch throat during creep exposure. The creep rupture life under multiaxial conditions has been predicted using FE analyses by employing Cocks and Ashby model and ductility exhaustion model. The predictions from the FE models are compared with the experimental data of the material from previous research [23].

## MATERIAL MODEL

In this work, P91 material has been used. Fig. 1 shows the true stress strain curve of P91 material at 25°C and 600°C. The tensile deformation shows a significant decrease at high temperatures compared to the one at room temperature. Creep properties of ex-service material were obtained from experimental data and analyzed with available literature as discussed in [12]. The creep properties based on low stress and high stress region were tabulated in Tab. 1.  $A$  and  $n$  are denoted as stress coefficient and stress exponent, respectively. The  $A_A$  and  $n_A$  are denoted as average stress coefficient and average stress exponent, respectively where the application of average creep strain rate may be effective in accounting for all three creep stages. The creep ductility of P91 material has shown a wide scatter over the wide range of stress [12]. The estimated creep ductility of 30% and 12% have been used in the FE analysis as the upper and lower bound value, respectively.

Region	$A(MPa^n/b^t)$	$n$	$A_A (MPa^n/b^t)$	$n_A$
High stress ( $\sigma > 130$ MPa)	$1.0 \times 10^{-33}$	13	$2.0 \times 10^{-31}$	13
Low stress ( $\sigma < 130$ MPa)	$2.0 \times 10^{-18}$	6	$2.0 \times 10^{-20}$	7

Table 1: Creep properties based on low stress and high stress regions at 600°C [12].

## FINITE ELEMENT MODEL

A two-dimensional axisymmetric (2D) finite element model of a notched bar specimen was modelled using Abaqus v6.12. One-quarter of the specimen was modelled taking into the advantage of the symmetry of the specimens as shown in Fig. 2. The specimen was modelled using four-node axisymmetric elements with reduced integrations (CAX4R). The mesh sensitivity analysis has been performed on three different three mesh densities. The more refined mesh had an influence on the predicted rupture time. However, in order to reduce the computational time, the most optimal refined mesh with the total number of nodes, 16803 and the total number of element, 16434 were used. The model has meshed in two major sections with a finer mesh around the notch throat as shown in Fig. 3. The smallest element size ahead of the notch root is 0.02 mm x 0.03 mm. The boundary condition was applied as shown in Fig. 2 where the nodes along the bottom face were strained in the  $y$ -direction. The uniform stress was applied along the top face of the model such that the desired net section stress across the throat is achieved.

## CREEP DAMAGE MODEL

A ductility exhaustion approach is used to calculate the creep damage during the finite element analysis. A damage parameter,  $\omega$  is adjusted in the range from 0 to 1, where damage occurs when =1. The accumulated damage rate is defined as the creep strain rate divided by the multiaxial creep ductility and is given by Eqn. (1) [24].

$$\omega = \frac{\dot{\varepsilon}^c}{\varepsilon_f^*} \quad (1)$$

where  $\dot{\varepsilon}^c$  is the creep strain rate and  $\varepsilon_f^*$  is the multiaxial creep ductility. The total damage at any time is the integral of the damage rate and can be expressed by Eqn. 2 [24].



$$\omega = \int_0^t \dot{\omega} dt \quad (2)$$

In this work, the Cocks and Ashby model [20] was employed to account for the material's creep ductility under multiaxial stress states. The model demonstrates that the ratio of multiaxiality and uniaxial ductility, is associated with hydrostatic stress,  $\sigma_m$ , and the equivalent stress,  $\sigma_e$ , which is commonly referred to as triaxiality. The stress triaxiality in the model is determined by the ratio of the mean stress to the von mises stress, and Eqn. (3) [24] describes the ratio of uniaxial to multiaxial creep ductility. The user subroutine USDFLD was used to implement this equation in the ABAQUS code.

$$\frac{\dot{\varepsilon}_f^c}{\dot{\varepsilon}_f^*} = \sinh \left[ \frac{2(n-0.5)}{3(n+0.5)} \right] / \sinh \left[ \frac{2(n-0.5)}{(n+0.5)} \frac{\sigma_m}{\sigma_e} \right] \quad (3)$$

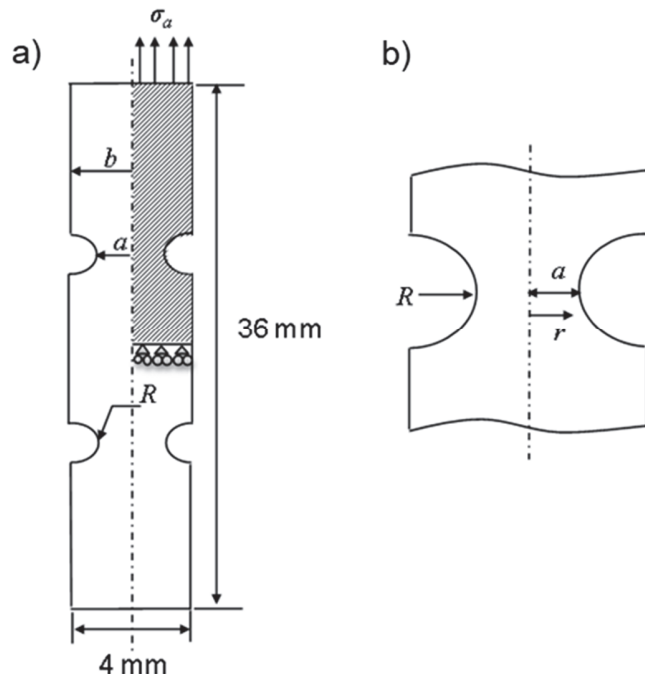


Figure 2: Illustration of notched bar specimen; a) complete specimen, b) feature of notch throat

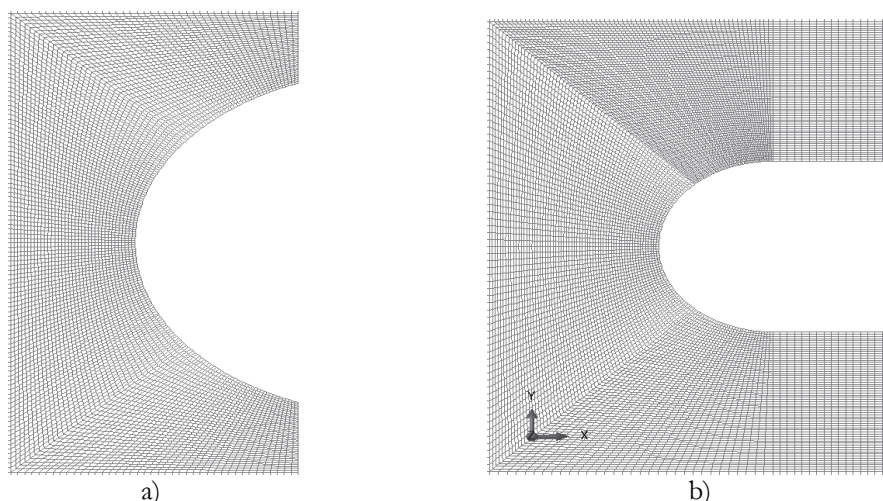


Figure 3: FE Mesh; a) Blunt notch, b) Medium Notch.

## NOTCHED SIMULATION RESULTS

### Stress distributions

The stress distributions throughout the notch throat in the notched bar analysis are not uniform. A normalized distance from the notch root is required to determine stress distribution throughout the notch throat. Fig. 4 to 6 show the von-Mises stress,  $\sigma_v$ , maximum principal stress,  $\sigma_I$ , and hydrostatic stress,  $\sigma_m$ , distribution, respectively across the notch throat from the initial loading until steady-state life as a function of normalized distance from the notch root,  $r/a$ . The normalized distance is shown from the center of the specimen where  $r/a=0$  is at the center and  $r/a=1$  is at the notch root.

From Fig. 4 it can be seen that after loading during the creep exposure the von-Mises stress is highest at the notch root for both notch types. As the creep deformation takes place, stress redistribution across the notch throat was found to change with creep exposure and approach stationary state. The stress redistributes and achieves its steady state after 42 h of creep exposure. At the center of the notch,  $r/a=0$ , the von Mises stress was significantly lower than that of 0.2% proof stress of P91 material (287 MPa). At the notch root  $r/a=1$ , the von Mises stress is still lower than the 0.2% proof stress, suggesting that the localized plastic deformation at the notch root does not contribute to the stress distribution across the notch throat from the beginning of creep loading for this material [6]. It is also seen in Figs. 4 (a) and (b) that the von-Mises stress is lower than that of the net stress for both notch acuity at steady-state life which may indicate the notch strengthening effect, as observed experimentally [6][25]. In general, it has been shown that von Mises stress regulates the creep deformation and the creep cavity nucleation processes, maximum principal stress regulates stress-directed diffusion-controlled intergranular cavity growth, and hydrostatic stress regulates continuum cavity growth [25]. It is envisaged that the presence of relatively uniform von Mises stress across the notch plane will result in more or less uniform transgranular creep cavity nucleation across the notch plane, depending on the degree of uniformity of the von Mises stress [24].

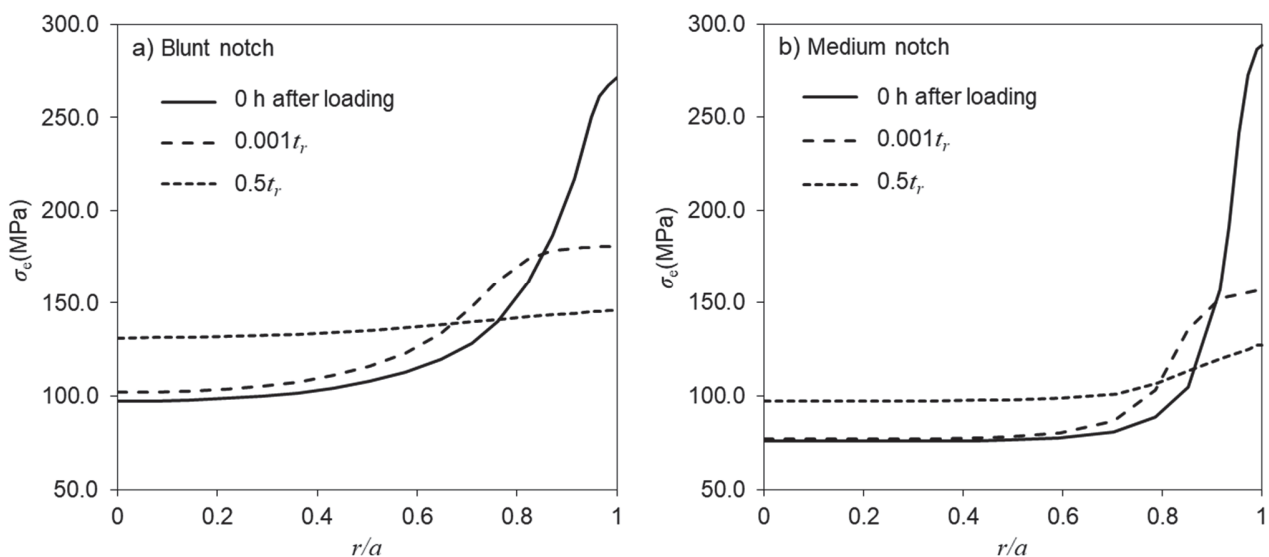


Figure 4: Von Mises stress distribution for a blunt and medium notch at net stress 187 MPa

The distribution of maximum principal stress  $\sigma_I$ , across the notch throat for the blunt and medium notch is shown in Figs. 5 (a) and (b), respectively. As shown in Fig. 5 (a) after reaching steady-state life, the maximum principal stress distribution shows a maximum value at  $r/a \sim 0.6$  which is more than the net stress for a blunt notch type. For the medium notch specimen (Fig. 5(b)), the peak of maximum principal stress occurred closer to the notch root. The hydrostatic stress,  $\sigma_m$  distribution across the notch throat for the blunt and medium notch is shown in Figs. 6 (a) and (b), respectively. The hydrostatic stress distribution shows similar behavior to that of the maximum principal stress. The hydrostatic stress remained below the net stress for both notches.

One of the factors that influence creep-rupture behaviour under multi axial stress states is triaxiality. Triaxiality is defined as the ratio of hydrostatic stress,  $\sigma_m$  and von Mises stress,  $\sigma_v$ . Fig. 7 shows the variation of triaxiality across the notch throat for the blunt and medium notch. It can be seen in Fig. 7 that the triaxiality is maximum at notch throat distance of



$r/a=0.5$  for blunt notch whereas the triaxiality is maximum near the notch root i.e.  $r/a=0.8$  for the medium notch. The medium notch has a maximum value of triaxiality nearly twice of the blunt notch. For both notch types, the triaxiality across the notch throat is significantly higher than that for a uniaxial test specimen,  $\sigma_m/\sigma_e=1/3$ .

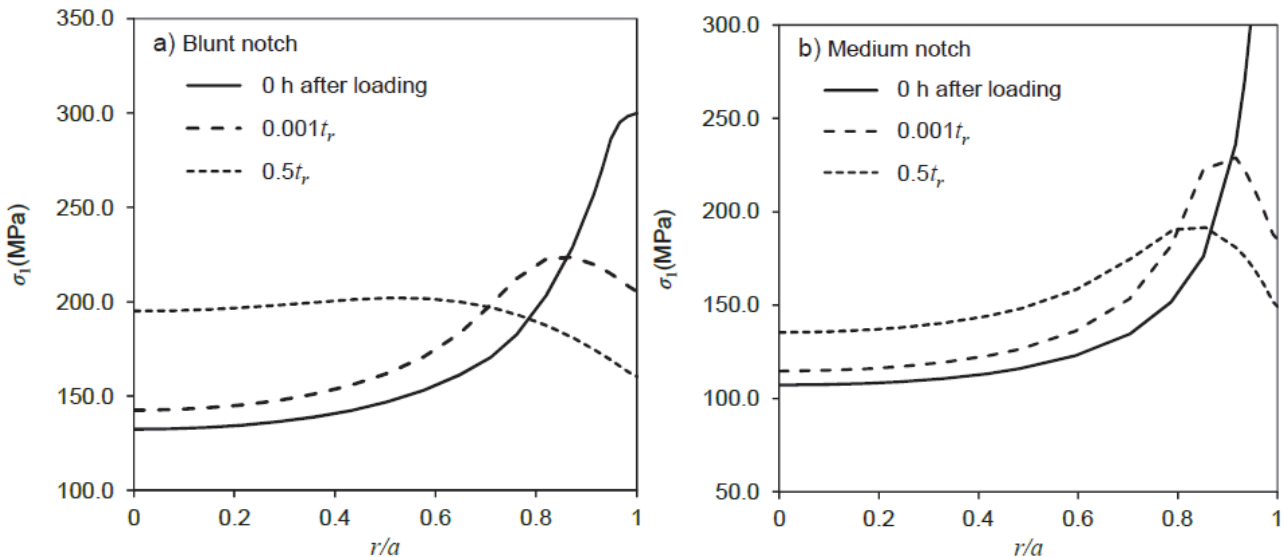


Figure 5: Maximum principal stress distribution for blunt and medium notch net stress = 187 MPa

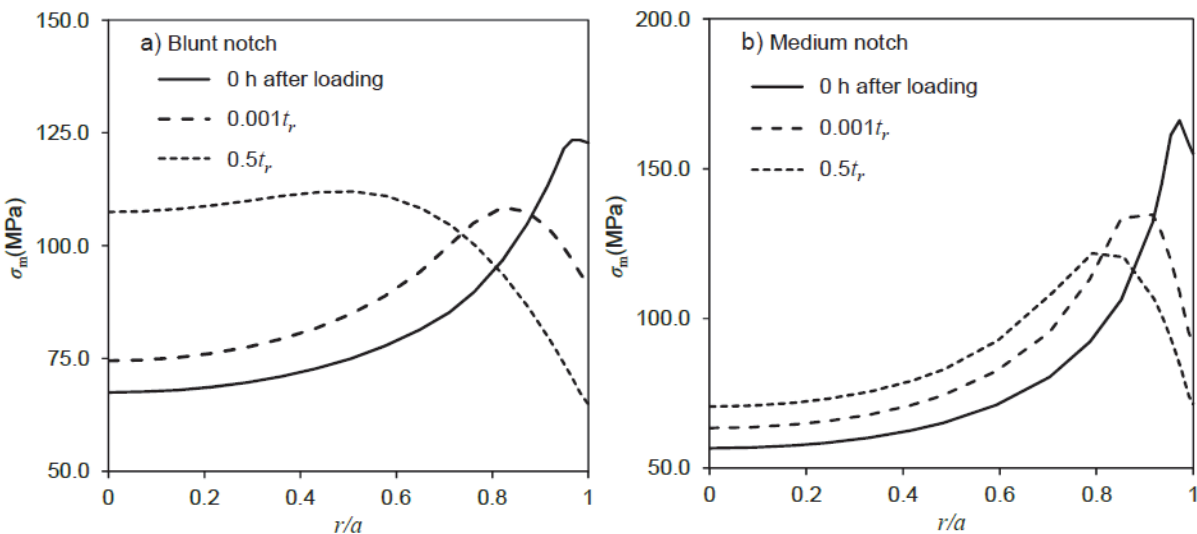


Figure 6: Hydrostatic stress distribution for blunt and medium notch bar at net stress = 187 MPa.

### Creep damage

In order to evaluate the creep damage accumulation, the FE analysis used a ductility exhaustion approach with the Cocks and Ashby damage model. The damage is calculated when the element attains  $\omega=1.0$ . The predicted time to rupture was taken when a few elements reach  $\omega=1.0$ . Two-dimensional contour plots of creep damage across the notch throat for blunt and medium notch are shown in Figs. 8 (a) and (b), respectively. The blunt notch shows the most uniform widespread of damage and the medium notch shows the most localized damage. The maximum damage is observed to occur near the notch root at first and then shifts toward the notch subsurface as it reaches a steady-state as shown in Fig. 8. In Fig. 8, the location of damage starts at the notch root from the beginning until the time to failure which is similar to the micrograph seen in the test specimen [12]. The most severe region of damage is seen along the notch throat for both types of the notch.

Fig. 9 shows the evolution of damage for both notch acuties for the net stress = 187 MPa. Damage evolutions across the notch are shown at  $0.25 t_r$ ,  $0.5 t_r$ , and  $t = t_r$ , where  $t_r$  is rupture time. It can be seen that the damage accumulation at each element across the notch throat increases over time. It can also be seen that the point at which damage first occurs is closer to the notch root for the medium notch than for the blunt notch. This is expected given that the maximum triaxial stress state is closer to the notch surface for the medium notch than for the blunt notch. Similar behaviour has been reported for P92 steel [26] where an increase in notch acuity results in the damage location moving closer to the notch root.

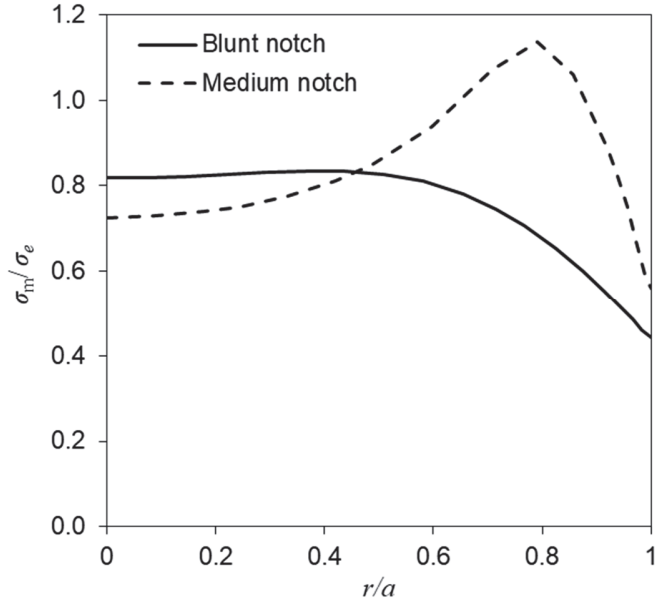


Figure 7: Variation of triaxiality across the notch throat for the blunt and medium notch at  $t = 0.5t_r$ .

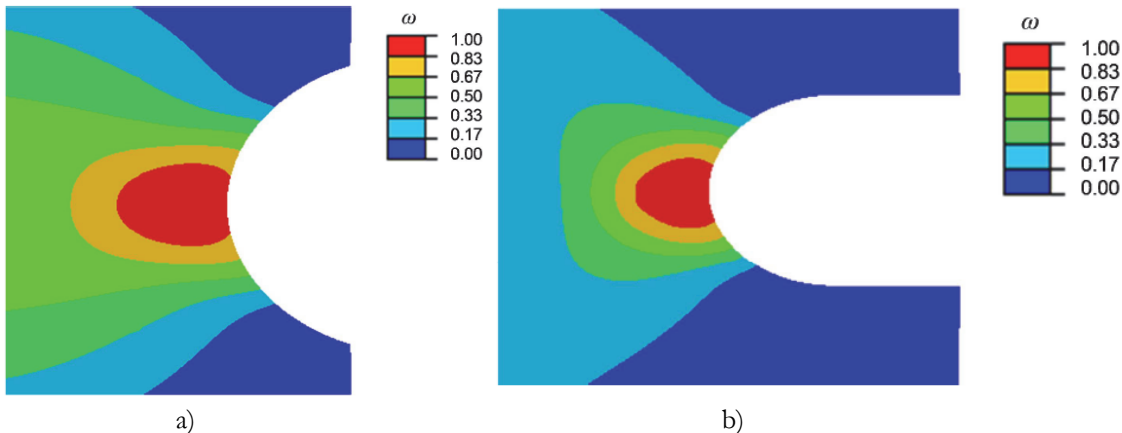


Figure 8: Creep damage contour at net stress = 187 MPa at  $t = 0.5t_r$  for a) blunt and b) medium notched

#### *Prediction of rupture time*

In this work, the predictions of rupture time were based on FE analysis coupled with Cocks and Ashby model. The rupture times were predicted when the few elements attain the damage,  $\omega = 1$ . It is shown that the prediction of the rupture time using Cocks and Ashby model in Eqn. (3) is strongly dependent on the creep ductility. To predict the rupture time, the lower and upper bound creep ductility of 12% and 30%, respectively, have been used in the FE.

Fig. 10 (a) and (b) shows of prediction of rupture time plot with net stress for the blunt and medium notch, respectively. The uniaxial and notched bar test data were also plotted in the same figures. The regression lines have been included for all the notches. It can be seen in both figures, the rupture life of notched specimens is higher than that of uniaxial specimens indicating the notch strengthening effect as observed experimentally. It is expected that with increasing notch acuity the rupture life increases hence the notch strengthening is enhanced.



The Cock and Ashby model has been utilized to predict the rupture life by using the lower and upper bound creep ductility of 12% and 30%, respectively. It can be seen in Fig. 10 (a) that for the blunt notch, lower bound creep ductility (0.12) predicts the rupture life better than upper bound creep ductility (0.30). The prediction of the long-term rupture life for the blunt notch specimen seems to coincide with the uniaxial data which may indicate that in long-term test data the blunt notch may exhibit similar behavior to that of the uniaxial specimen. For the medium notched in Fig. 10 (b), the upper bound creep ductility predicts the rupture life better than the lower bound creep ductility. At the same net stress, the medium notches always have a longer predicted lifetime than the blunt notch.

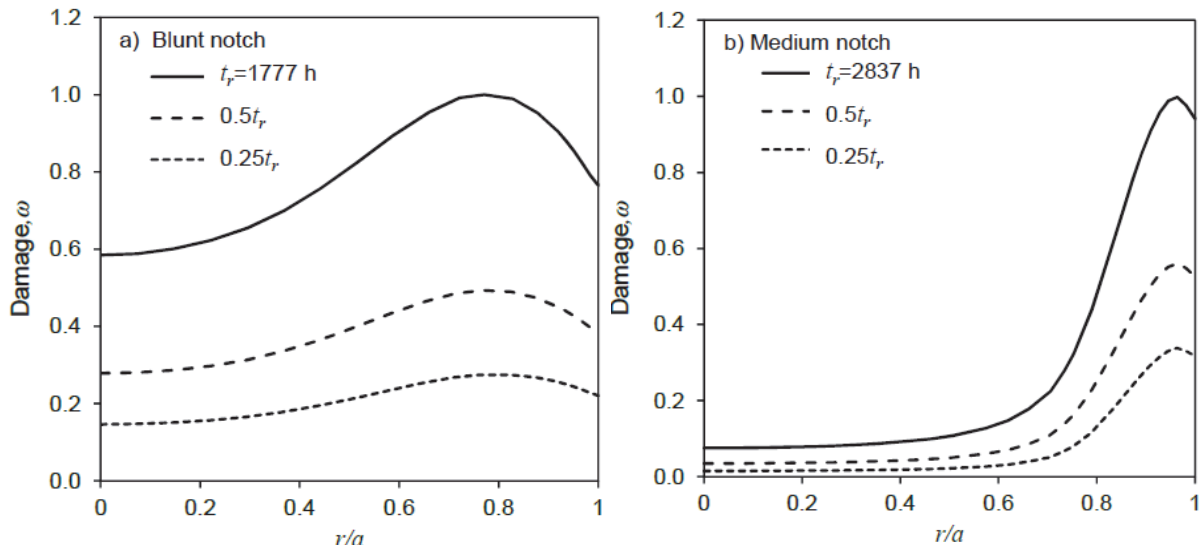


Figure 9: Damage evolution across the notch throat at net stress of 187 MPa for a) blunt notch and b) medium notch

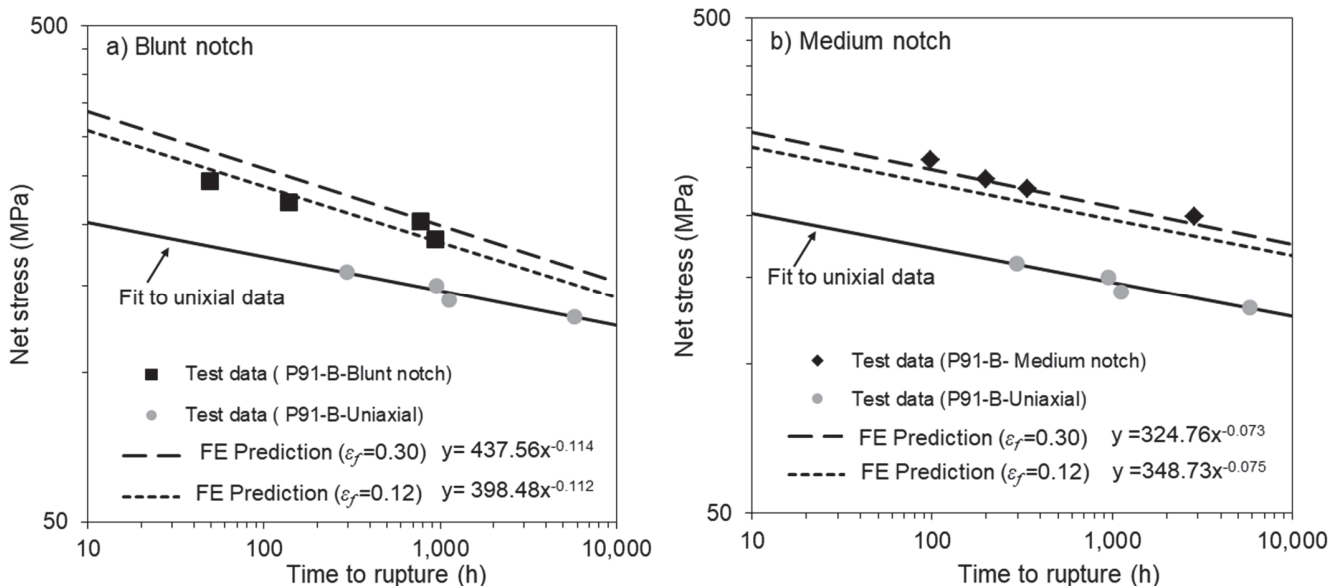


Figure 10: FE Prediction of rupture life using  $\varepsilon_f = 0.30$  and 0.12 for a) blunt notch and b) medium notch.

## CONCLUSIONS

The FE analyses have been performed on P91 material for the blunt and medium notched bar. A ductility exhaustion model has been used within the FE model by employing the Cocks and Ashby model.

- The stress distribution for blunt notched specimens showed a more uniform distribution compared to the



medium notched specimen. The von Mises stress is lower than the net stress for both notch acuity which indicates the notch strengthening effect as observed experimentally.

- As defined in the Cocks and model, the triaxiality contributes to the creep rupture behaviour under a multiaxial stress state. It is shown that the triaxiality is maximum at notch throat distance of  $r/a = 0.5$  for blunt notch whereas the triaxiality is maximum near the notch root, i.e  $r/a=0.8$  for the medium notch. The medium notch has a maximum of triaxiality nearly twice of the blunt notch.
- Creep damage evolution has shown that the blunt notch shows the most uniform widespread of damage and the medium notch show the most localized damage
- Creep ductility of 12% and 30% predicts the rupture life well for blunt and medium notched bars, respectively.

## REFERENCES

- [1] Al-Faddagh, K.D., Webster, G.A., Dyson, B.F. (1984). Influence of state of stress on creep failure of 2 1/4% Cr1% Mo steel. *Mechanical Behaviour of Materials*, pp. 289–95.
- [2] Wu, D., Christian, E.M., Ellison, E.G. (1984). Influence of constraint on creep stress distribution in notched bars, *J. Strain Anal. Eng. Des.*, 19(4), pp. 209–20.
- [3] Hayhurst, D.R., Henderson, J.T. (1977). Creep stress redistribution in notched bars, *Int. J. Mech. Sci.*, 19(3), pp. 133–46.
- [4] Goyal, S., Laha, K., Das, C.R., Panneerselvi, S., Mathew, M.D. (2014). Effect of Constraint on Creep Behavior of 9Cr-1Mo Steel, *Metall. Mater. Trans. A*, 45(2), pp. 619–32, DOI: 10.1007/s11661-013-2025-z.
- [5] Chang, Y., Xu, H., Ni, Y., Lan, X., Li, H. (2015). The effect of multiaxial stress state on creep behavior and fracture mechanism of P92 steel, *Mater. Sci. Eng. A*, 636, pp. 70–6.
- [6] Goyal, S., Laha, K., Mathew, M.D. (2014). Creep Life Prediction of Modified 9Cr-1Mo Steel under Multiaxial State of Stress, *Procedia Eng.*, 86, pp. 150–7, DOI: 10.1016/j.proeng.2014.11.023.
- [7] Wasmer, K., Biglari, F., Nikbin, K.M. (2002). Multiaxial failure behaviour in advanced steels at elevated temperatures. *Proceedings of the ECF 14 Conference, Krakow*, pp. 553–62.
- [8] Dyson, B.F., Loveday, M.S. (1981). Creep fracture in Nimonic 80A under triaxial tensile stressing. *Creep in structures*, Springer, pp. 406–421.
- [9] Xu, X., Wang, G.Z., Xuan, F.Z., Tu, S.T. (2016). Effects of creep ductility and notch constraint on creep fracture behavior in notched bar specimens, *Mater. High Temp.*, 33(2), pp. 198–207.
- [10] Hayhurst, D.R. (1972). Creep rupture under multi-axial states of stress, *J. Mech. Phys. Solids*, 20(6), pp. 381–382, DOI: 10.1016/0022-5096(72)90015-4.
- [11] Maleki, S., Mehmanparast, A. (2013). Creep Crack Growth Prediction of Very Long Term P91 Steel Using Extrapolated Short-Term Uniaxial Creep Data, *ASME Press. Vessel Pip. Conf. Proc.*, 97506.
- [12] Norhaida Ab Razak. (2018). Creep and Creep-Fatigue Interaction in New and Serviced Exposed P91 Steel. *Imperial College London*.
- [13] Abe, F. (2020). Creep rupture ductility of Gr. 91 and Gr. 92 at 550° C to 700° C, *Mater. High Temp.*, 37(4), pp. 243–255.
- [14] Zhang, J.W., Wang, G.Z., Xuan, F.Z., Tu, S.T. (2015). Effect of stress dependent creep ductility on creep crack growth behaviour of steels for wide range of C, *Mater. High Temp.*, 32(4), pp. 369–376.
- [15] Zhou, H., Mehmanparast, A., Nikbin, K. (2021). Determination of long-term creep properties for 316H steel using short-term tests on pre-strained material, *Exp. Tech.*, 45(4), pp. 549–60.
- [16] Kachanov. (1999). Rupture time under creep conditions, *Int. J. Fract.*, (97), pp. 11–8.
- [17] Hyde, T.H., Sun, W., Becker, A.A. (2000). Failure prediction for multi-material creep test specimens using a steady-state creep rupture stress, *Int. J. Mech. Sci.*, 42(3), pp. 401–423, DOI: 10.1016/S0020-7403(99)00008-9.
- [18] Spindler, M.W. (2004). The multiaxial creep ductility of austenitic stainless steels, *Fatigue Fract. Eng. Mater. Struct.*, 27(4), pp. 273–281, DOI: 10.1111/j.1460-2695.2004.00732.x.
- [19] Isobe, N., Yashirodai, K., Murata, K. (2014). Creep damage assessment for notched bar specimens of a low alloy steel considering stress multiaxiality, *Eng. Fract. Mech.*, 123, pp. 211–22.
- [20] Cocks, A.C.F., Ashby, M.F. (1982). On creep fracture by void growth, *Prog. Mater. Sci.*, 27(3–4), pp. 189–244, DOI: 10.1016/0079-6425(82)90001-9.
- [21] Jiang, Y.P., Guo, W.L., Yue, Z.F., Wang, J. (2006). On the study of the effects of notch shape on creep damage development under constant loading, *Mater. Sci. Eng. A*, 437(2), pp. 340–347.



- [22] Yatomi, M., Nikbin, K.M., O'Dowd, N.P. (2003). Creep crack growth prediction using a damage based approach, *Int. J. Press. Vessel. Pip.*, 80(7–8), pp. 573–583, DOI: 10.1016/S0308-0161(03)00110-8.
- [23] Razak, N.A. (2021). Experimental Study of Multiaxial Stress State on Creep Rupture Life and Ductility of P91 Steel, *J. Fail. Anal. Prev.*, 21(6), pp. 1991–1999.
- [24] Webster, G.A., Ainsworth, R.A. (1994). High Temperature Component Life Assessment, .
- [25] Nix, W.D., Earthman, J.C., Eggeler, G., Ilschner, B. (1989). The principal facet stress as a parameter for predicting creep rupture under multiaxial stresses, *Acta Metall.*, 37(4), pp. 1067–1077.
- [26] Ni, Y.Z., Lan, X., Xu, H., Mao, X.P. (2014). Finite element analysis and experimental research on notched strengthening effect of P92 steel, *Mater. High Temp.*, 31(2), pp. 185–190, DOI: 10.1179/1878641314Y.0000000010.